Flow Measurement and Instrumentation 44 (2015) 19–26

Contents lists available at ScienceDirect

Flow Measurement and Instrumentation

journal homepage: www.elsevier.com/locate/flowmeasinst

Improvements to NIST'S air speed calibration service

Iosif I. Shinder*, Christopher J. Crowley, B. James Filla, Michael R. Moldover

Sensor Science Division, National Institute of Standard and Technology, Mail Stop 8361, 100 Bureau Drive, Gaithersburg, MD 20899-8361, USA

ARTICLE INFO

Available online 8 December 2014

Keywords:
Airspeed measurements
Primary standard
Wind tunnel

ABSTRACT

We discuss five significant improvements to the Air Speed Calibration Service conducted by the National Institute of Standards and Technology (NIST): 1. Reduced-uncertainty calibration of the secondary standard [Laser Doppler Anemometer, (LDA)] using a spinning disk, 2. Reduced-uncertainty LDA measurements that account for the position-dependence of the air speed in the test section and for window effects, 3. Improved repeatability, precision, and ease of calibrations by using automated data acquisition and PID air speed control, 4. optical character recognition data acquisition system for anemometers lacking electrical outputs, and 5. up-to-date uncertainty budget of the LDA. Also, we present the results (with uncertainties) of Pitot tube calibrations.

Published by Elsevier Ltd.

1. Introduction

In 2007, Yeh and Hall described the operating principles, traceability chain, and uncertainties of NIST's air speed calibration facility in detail. [1] Recently, we reviewed the traceability chain and made hardware and software changes to automate the data acquisition, thereby improving the efficiency of the calibration facility. While making these changes, we discovered and solved several measurement problems that were not discussed by Yeh and Hall. Here, we report the following 5 improvements: (1) reduced-uncertainty calibration of the secondary standard [Laser Doppler Anemometer, (LDA)] using a spinning disk; (2) reduced-uncertainty LDA measurements that account for the position-dependence of the air speed in the test section and for window effects; (3) improved repeatability, precision, and ease of calibrations by using automated data acquisition and PID air speed control; (4) optical character recognition data acquisition system for anemometers lacking electrical outputs; and (5) up-to-date uncertainty budget for the calibration of the LDA. In the future, we will incorporate these improvements in a revision of Ref. [1]. The revision will also include many uncertainty components that are not discussed here because they have not changed significantly. Then, the revision of Ref. [1] will include a complete uncertainty analysis of NIST's modernized air speed calibration facility.

2. NIST's wind tunnel

NIST's Air Speed Calibration Facility is a closed-loop wind tunnel with length of 43.5 m and a width 8.9 m. (See Fig. 1 and [1, 2].) The wind tunnel has two interchangeable test sections, each 12.1 m long. The minimum air speed is 0.2 m/s for both sections. Both test sections provide longitudinal free-stream turbulence levels of 0.07% over most of the air speed range and a transverse velocity gradient of less than 1% within a working area that spans 90% of the cross-sectional areas. The maximum air speeds are 45 m/s in the taller test section and 75 m/s in the contracted section. The contracted test section is 1.2 m high and 1.5 m wide and the taller test section is 2.1 m high and 1.5 m wide.

In order to trace a measurement (such as air speed) to the International System of Units, (SI), either the definition of the measured quantity must be realized or a complete chain of calibrations must be established tracing the measured quantity back to the seven fundamental quantities in the SI. Because it is impractical to determine air speed by directly measuring length and time, practical air speed measurements use calibrated anemometers (i.e. air speed meters). Air speed measurements traceable to the SI are established by calibrating an anemometer at a facility such as NIST's which traces its calibrations to length and time standards. NIST uses a spinning disk as a traceable-to-the-SI velocity standard. NIST calibrates a laser Doppler anemometer (LDA) as a working standard in the airspeed range from 0.2 m/s to 75 m/s. In the future, NIST will use a Pitot tube as a check (or tertiary) standard for measuring air speeds ranging from 5 m/s to 75 m/s under low-turbulence conditions.

3. Sources of uncertainty

Fig. 2 illustrates the propagation of uncertainties connected to air speed measurements. Both working standards (LDA and Pitot tube) provide calibrations with expanded uncertainty approximately 0.4% in the range specified above. (Unless stated otherwise, all

* Corresponding author.
E-mail address: Iosif.Shinder@nist.gov (I.I. Shinder).

http://dx.doi.org/10.1016/j.flowmeasinst.2014.11.005
0955-5986/Published by Elsevier Ltd.

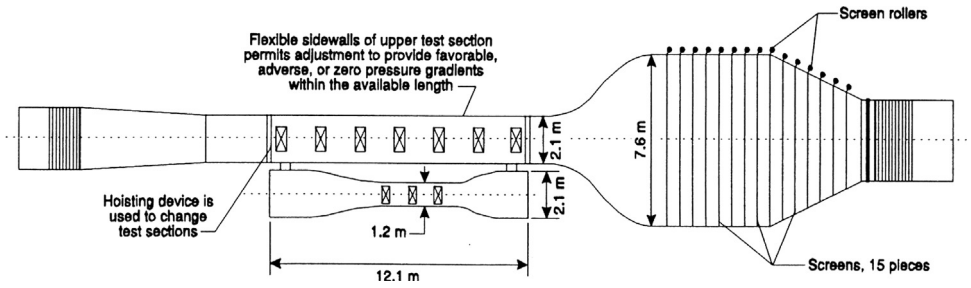

Fig. 1. Side view of interchangeable test sections.

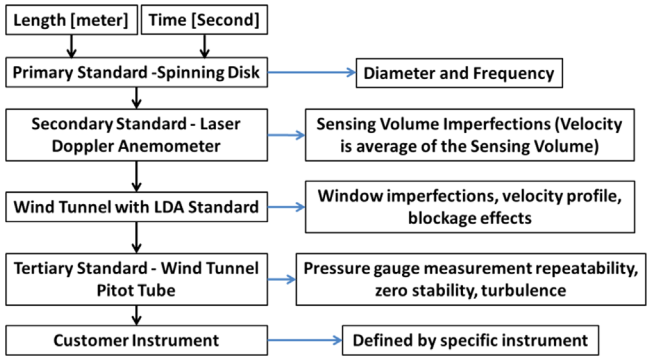

Fig. 2. Calibration chain and the associated sources of uncertainty.

uncertainties are expanded standard uncertainties with coverage factor $k=2$ that corresponds to a 95% confidence interval.)

4. Realizing the primary standard

The two conventional methods of tracing air speed measurements to length and time standards are:

(1) An air-speed sensor is moved through stationary air at a known velocity. This method can be realized by either linear or rotational movement.
(2) The velocity of particles entrained in the air flow is measured using optical or other means. The optical (or other) system is calibrated with a mechanical device, such as a spinning disk, that simulates the moving particles.

The first method requires some corrections because the still air is disturbed and secondary flows are created by the movement of the sensor and its support. The first method has been used by other laboratories to calibrate secondary standards such as an LDA, a Pitot tube, a hot wire anemometer, *etc*. Ref.[3,4]. NIST realizes the second method by calibrating an LDA using a spinning disk that has well-known dimensions and a stable, measured rotational speed. (See Fig. 3.) When calibrating the LDA, we scatter the crossed laser beams off a 5 μm-diameter wire that was attached to the spinning disk. (The scattering from the wire simulates the scattering from tracer particles flowing through the sensing volume.) After the LDA is calibrated, NIST uses it to characterize the wind tunnel, calibrate customers' instruments, and to calibrate Pitot tubes that are used as tertiary, working standards to perform routine air speed calibrations. For more details about spinning disk calibrations, see Ref. [5–7].

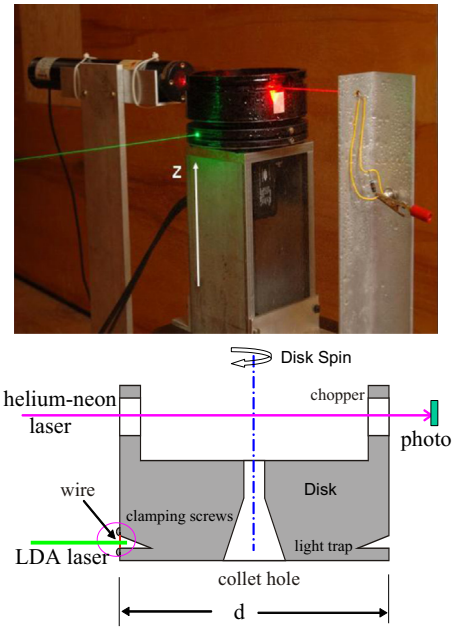

Fig. 3. Photograph and drawing of spinning disk used to calibrate LDA.

5. Calibrating the LDA

NIST's LDA determines one component of the velocity of objects moving through a sensing volume that is defined by the overlap of two focused laser beams. In the overlap region, the two beams form interference fringes with a precisely defined spacing that establishes the length scale for the air-speed measurement. Ideally the focused laser beams overlap exactly at their waists and the fringe-filled overlap volume has the approximate shape of a biaxial ellipsoid. As tracer particles (*e.g.* oil droplets) flowing with the air in the wind tunnel pass through the fringes in the sensing volume, they are alternately brightly and dimly illuminated; therefore, they appear to "blink" on and off. A burst spectrum analyzer (BSA) measures the blinking rate which defines the time scale for LDA air speed measurements.

The sensing volume will be well defined and symmetrical only after rigorous adjustment of the optics by an experienced technician using special instruments and optics; thus, it is usually done by the manufacturer and its cost is a significant fraction of the cost of a new LDA system. In some cases (for example, fiber optics probes), no adjustment is possible. Even after adjustment, the geometry of the optical system may drift with time, causing the shape of the sensing volume to lose its symmetry.

Imperfections of the quality and symmetry of the sensing volume will adversely affect the transfer of the SI unit of velocity from the spinning disk to the LDA. Small departures from symmetry generate irregularity in calibration results; larger departures from symmetry, caused by poorly aligned LDA beams, can generate

sensing volumes that contain major defects such as insensitive holes that do not contain interference fringes. If such defects are present, attempts to align the spinning disk and the LDA may produce erratic, unrepeatable, and puzzling results such as changes in the sign of the derivative of the LDA reading with respect to position [6].

NIST began using an LDA in 1999 [5]. At that time, LDA data were analyzed by assuming that the sensing volume was symmetrical and the beams crossed at their waists. The position of the center of the sensing volume relative to the fine wire on the spinning disk was assumed to be the mid-point between the two locations at which the LDA signal disappeared. This protocol was carried out with a precision of a fraction of a millimeter and led to an LDA calibration uncertainty on the order of 1%.

In 2010 NIST adopted another protocol. The center of the sensing volume was defined with a precision of 0.1 mm by the symmetry of the signal from the burst spectrum analyzer [2] at two velocities: 10 m/s and 20 m/s. Then, this position was used to measure all other velocities. This protocol led to an LDA calibration uncertainty of 0.4%. Although 2010 definition is more precise than the 1999 definition, it does not guarantee that the sensing volume is symmetrical nor does it allow for velocity-dependent changes in the position of the wire relative to the sensing volume. Velocity-dependent changes will occur if the wire's shape is changed (by changing centrifugal and/or drag forces) or if the axis of the spinning disk is changed by velocity-dependent wobbling or vibration. When such velocity-dependent changes are ignored, the LDA calibration will appear to be velocity dependent. Because the 1999 LDA calibration data were more precise at the higher velocities, they were weighted more heavily in determining a velocity-dependent calibration curve and the deviations from linearity at low velocities were treated as a velocity-dependent uncertainty [1].

In 2011, NIST revised the protocol for LDA calibrations a third time [6]. The 2011 protocol integrates the weighted LDA velocity measurements and position of the wire over the entire sensing volume at *every* velocity. To conduct the integration, the LDA optical probe was mounted on an automated traverse system that moved the laser sensing volume relative to the wire. Fig. 4 shows the velocity indicated by the LDA as a function of the LDA position relative to the spinning disk. The indicated velocity curve has a characteristic shape that is independent of velocity throughout the range 0.2 m/s to 10 m/s.

Fig. 5 shows the number of bursts registered by the burst spectrum analyzer as a function of the position of the LDA. The plot has a well-defined rectangular shape with no voids inside the sensing volume. Above 20 m/s, the spinning disk vibrates and the

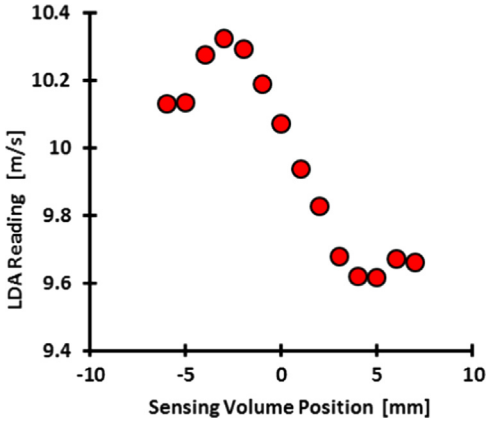

Fig. 4. LDA reading vs position at 10 m/s. These data were acquired while implementing the 2011 protocol.

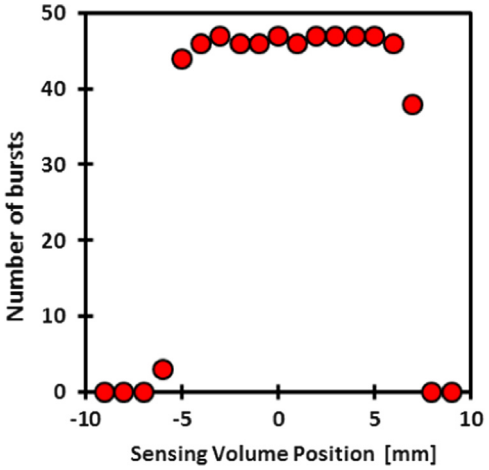

Fig. 5. Number of bursts vs position at 10 m/s.

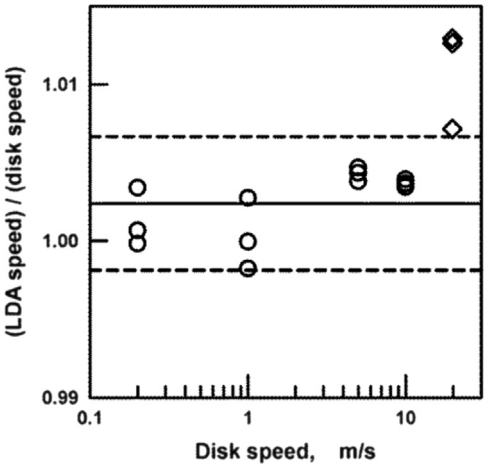

Fig. 6. Calibration of the LDA with the spinning disk. For the data from 0.2 m/s to 10 m/s (circles), the lines represent the mean m and $m \pm 2\sigma$. Data at 20 m/s (diamonds) are not included in the mean.

plot is no longer rectangular. This time-consuming protocol accounts for velocity-dependent changes in the disk's rotation axis. As shown in Fig. 6, the LDA calibration coefficient is independent of the disk's velocity up to 10 m/s. The dashed lines in Fig. 6 bracket the mean calibration factor by ± 0.0043 which corresponds to ± 2 standard deviations. (At 20 m/s, the spinning disk vibrated and the apparent calibration factor changed.) The theory of the Doppler effect predicts that Doppler shift is a linear function of velocity of the moving object. Wind tunnel measurements are consistent with this prediction. [5,6,7] We rely on this linearity to apply LDA calibration factor between 20 m/s (where NIST's spinning disk begins to vibrate) and 75 m/s (the NIST wind tunnel maximum airspeed). Both the 2010 and 2011 protocols lead to an LDA calibration uncertainty of 0.4%; however, the 2011 protocol it is less sensitive to the gradual loss of symmetry of the sensing volume that occurs with age.

We note that the 2011 protocol is insensitive to possible velocity-dependent changes in the shape of the wire. If the light-scattering wire were replaced with a light-scattering scratch on the disk, such shape changes will not occur.

6. Velocity profile

Fig. 7 sketches the development of the velocity profile as the flow passes through the test section of the wind tunnel. At the

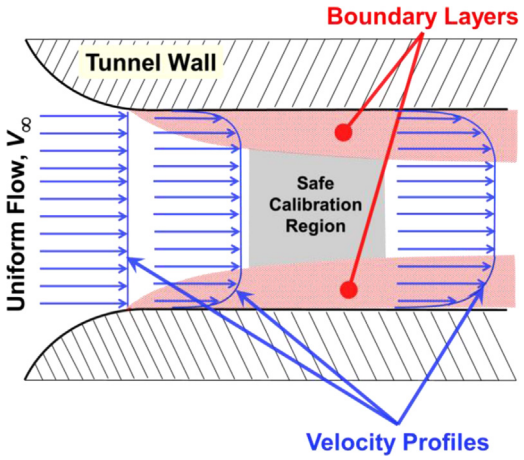

Fig. 7. The velocity profile develops as the air moves. downstream in the wind tunnel.

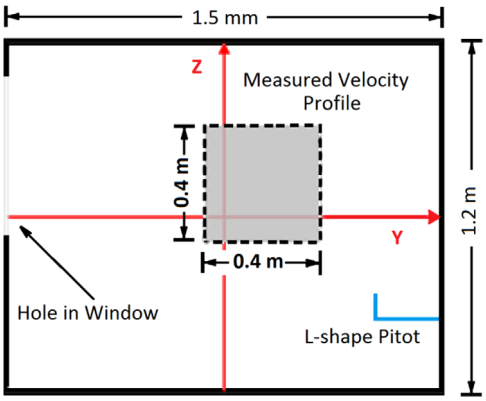

Fig. 8. Schematic of cross section of wind tunnel through the. "safe calibration region" at $X=0$ m. (The X-coordinate measures the distance along the wind tunnel's axis downstream from the LDA's sensing volume.).

flared entrance to the test section, the air speed is nearly independent of position; that is, the velocity profile is flat. As the flow proceeds downstream, boundary layers develop along the tunnel's walls, ceiling, and floor; the velocity-vs-position profile becomes curved; and the air speed in the center of the tunnel increases. NIST conducts its calibrations in the "Safe Calibration Region" near the center of the test section.

Fig. 8 is a cross section of the wind tunnel that passes through the "Safe Calibration Region". The initial position of the LDA sensing volume is the center of test section with the coordinates [$Y=0$, $Z=0$] in Fig. 8. We used a traverse system to scan the 40 cm × 40 cm area with the LDA shown by the gray square in Fig. 8. To avoid the effects of window imperfections discussed in the next section, the LDA light passed through a rectangular hole (50 cm tall and 10 cm wide) that we had cut in a Plexigass window in the side of the wind tunnel. We were concerned that the hole might affect the velocity profile; therefore, we covered most of the rectangular hole leaving a 10 cm × 10 cm opening. The profile did not change when we covered most of the hole. During the scan, we kept the air speed constant using a PID control loop linked to a Pitot tube placed on the side of the wind tunnel opposite the hole in the window shown in Fig. 8.

A typical velocity profile is displayed in Fig. 9. The maximum velocity difference from the center of the tunnel was approximately 0.1% in the vertical (Z) direction and 0.15% in the horizontal (Y) direction. The stability of the flow was better than 0.05% for air speeds from 5 m/s to 20 m/s.

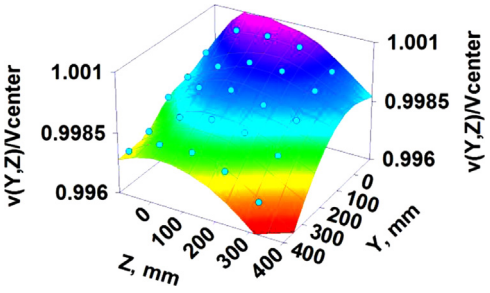

Fig. 9. Velocity profile at 10 m/s in the "safe calibration region" of Fig. 8.

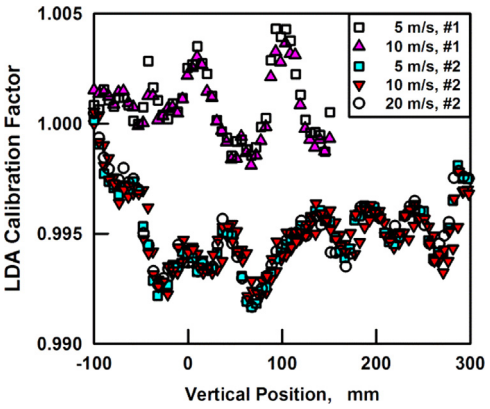

Fig. 10. Effect of two different Plexiglass windows on. the LDA calibration factor.

We did not measure the velocity profile below 5 m/s because the uncertainty of the Pitot tube measurements becomes as large or larger than the uncertainty of the velocity profile. Above 20 m/s, the increasing Reynolds number ensures that the velocity profile becomes increasingly flat.

7. Window imperfections

During our first attempts to measure the velocity profile, we found that the Plexiglass window has an effect on the LDA calibration factor. This effect was measured for two different windows (Fig. 10). Because the surfaces of the windows are neither flat nor parallel, the windows change the angle between the crossing laser beams and the positions of the beam's waists. As the sensing volume of the LDA was raised, the calibration factor varied by as much as 0.8%. For each window, the variation was reproducible and independent of the air speed. In order to circumvent this effect, we fixed the position of the LDA relative to the window so that the sensing volume is always located within ± 0.003 m of the centerline of the wind tunnel. Because the LDA is calibrated at this location with the spinning disk, the calibration reduces the impact of window effects to less than 0.05%.

8. Pitot tube as a tertiary standard

We mounted a 9 mm-diameter, L-shape Pitot tube 20 cm from the wall (Fig. 8) of the wind tunnel and calibrated it using the LDA. The following precautions were taken during Pitot tube installation: (a) Pitot tube was installed permanently, (b) position and distance from the wall was measured, (c) both yaw and pitch angles were set at zero values with uncertainties better than 1°. The errors due to angular misalignments are proportional to the cosine of the angles or approximately 0.02% of the air speed.

The calibration results taken in two measurement ranges (0.5 to 5 m/s and 5 to 75 m/s, Fig. 11) demonstrate that the Pitot tube can be used as a tertiary or "check" standard for air speeds above 2 m/s with only an insignificant increase in the measurement uncertainty over the LDA. We did not detect any time-dependence of the Pitot-tube calibration during a 10 day period. Between 5 m/s and 75 m/s, the expanded ($k=2$) uncertainty of this Pitot tube as a working standard is 0.41%.

9. Turbulence and pressure measurements

When Pitot tubes are used as transfer standards at low air speeds, the uncertainty of the air speed measurements is dominated by three phenomena: (1) zero drift of the differential pressure gauge, (2) noise in the differential pressure gauge, and (3) turbulence in the wind tunnel. We discuss these in turn.

(1) NIST uses a capacitance diaphragm gauge to measure differential pressures below 20 Pa. The manufacturer claims that the gauge's uncertainty is the larger of 0.2% of full scale or 0.04 Pa when the output is integrated for 0.4 s. These uncertainties are twice the differential pressure itself for an air speed of 0.2 m/s. Therefore, we reduced both uncertainties by increasing the integration time up to a practical limit of a few minutes. To separate the zero drift and noise of the capacitance diaphragm gauge from real fluctuations of the air speed, we conducted two different tests during which we simultaneously compared the outputs of two similar differential pressure gauges (MKS Model 698, 10 Torr range) while they were connected to the same inputs. The results of these tests are displayed as Youden plots in Fig. 12. During the first test, a short tube was used to connect the input of first gauge (P1) to the input of the second gauge (P2). A 6.4 h long test was then performed where readings from both gauges were taken every 4 min, resulting in 96 readings per gauge. Each reading was an average of 50,000 data points acquired over a 50 s interval (using a DAQ system sampling at 1 kHz). This replicates the procedure followed during the calibration of customer instruments, where 4 min elapses during a change in air speed. The resulting average readings and standard deviations for gauges P_1 and P_2 were (0.00002 ± 0.00099) Pa and (-0.00007 ± 0.00073) Pa, respectively. (See the upper panel of Fig. 12.)

(2) During a second 6.4 h-long test, both differential pressure gauges were connected to the same Pitot tube inside wind tunnel with zero flow. During the second test, P_1 and P_2 varied by ± 0.01 Pa; however, the average value and standard deviation of P_1-P_2 was (-0.00006 ± 0.00103) Pa. Thus, the zero drift of the differential pressure gauges was much smaller than the differential pressure produced by random air motion within the wind tunnel. We conclude that drift of the pressure-zero can be neglected during 4 min-long intervals between measurements.

(3) The effect of turbulence on calibrations is twofold: (a) it changes the total pressure in the flow and (b) it introduces noise in averaged calibration data which can be decreased by increasing the measurement time. We estimate the effect of changing of the total pressure in presence of turbulence by assuming that the total pressure is a sum of dynamic pressure and averaged pressure produced by turbulence [8]. For a turbulence level of 1% of the air speed, the turbulence pressure will be only the square of this value and additional pressure will be on the order of 0.01%. If the turbulence level reached 10%, it would change the Pitot calibration by approximately 1%. In order to estimate the effect of noise we assume that the random air motion that was present at zero air speed is also present at the air speed 0.2 m/s. This will be discussed in the next paragraph.

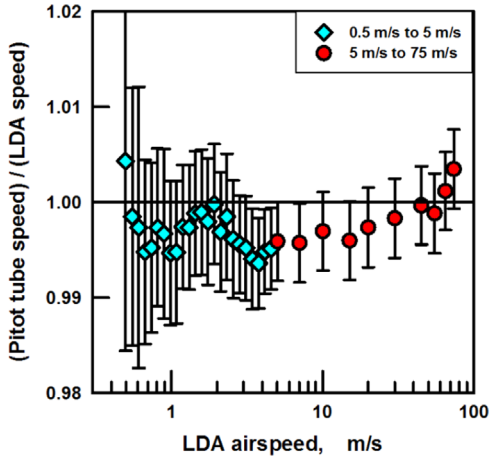

Fig. 11. Pitot tube calibration.

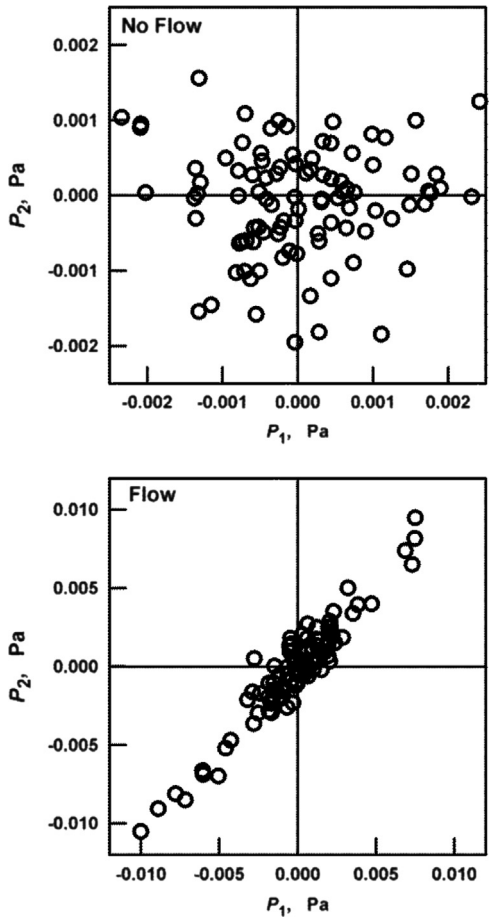

Fig. 12. Comparison of two differential pressure gauges. Top: both gauges are connected by a short tube. Bottom: both gauges are connected to the same Pitot tube. The scales on the top plot are expanded 5 × relative to the bottom plot.

10. Quantifying pressure fluctuations

Our improved air speed control and data acquisition software operates at rates up to 10 kHz. The differential pressure gauge (MKS Model 698) generates a voltage output with a minimum integration time of 4 ms which corresponds to a bandwidth of 250 Hz. During typical system operation, we digitize this output at a 1 kHz rate. The data is acquired at 10 Hz, in 100 point data

blocks, which are then averaged to yield 0.1 s interval mean values. The differential pressure fluctuations were measured at air speeds spanning the range 0.2 m/s to 75 m/s, corresponding to differential pressures ΔP spanning the range 0.02 Pa $< \Delta P <$ 3300 Pa. In order to minimize the effects of zero drift, the differential pressure gauge was re-zeroed for every calibration point for air speeds below 5 m/s. At each air speed, ΔP was measured 50,000 times during an interval of 50 s. Fig. 13 displays the standard deviation of the differential pressures $\sigma(\Delta P)$ from their mean values during 50 s intervals. Below 1 Pa (corresponding to ~1 m/s), $\sigma(\Delta P) \approx 0.008$ Pa; that is, the pressure fluctuations were a constant, independent of ΔP. Above 50 Pa (corresponding to ~10 m/s), $[[\sigma(\Delta P)]/\Delta P] \approx 0.002$ that is, the relative pressure fluctuations were a constant, independent of ΔP. (See Fig. 13.) For low air speeds ($\Delta P \leq 1$ Pa), we conjecture that flow-generated pressure fluctuations were much smaller than the pressure fluctuations present in the atmosphere. For high air speeds ($\Delta P \geq 50$ Pa), we conjecture flow-generated pressure fluctuations are much larger than the pressure fluctuations in the atmosphere.

Regardless of their origin, we treated the pressure fluctuations as two, uncorrelated, noise sources which must be added in quadrature

$$\sigma(\Delta P_{50}) = \sqrt{\sigma(\Delta P)^2_{\text{low-flow}} + \sigma(\Delta p)^2_{\text{hi-flow}}}$$
$$= \sqrt{(0.008\ \text{Pa})^2 + (\Delta P 0.0022)^2} \quad (1)$$

We obtained the numerical values in Eq. (1) by analyzing the data displayed in Fig. 13 and we attached the subscript "50" to ΔP_{50} to emphasize the numerical values are only correct for a 50 s averaging time. The Allan variance of the pressure readings had a minimum near 50 s. For longer averaging times, the drift of the pressure transducer's zero will increase the uncertainty of ΔP.

Using the density of ambient air, Eq. (1) can be rewritten in terms of air speed

$$u_r(V_{50}) = 10^{-4}\sqrt{\left(6.7\ \text{m}^2\ \text{s}^{-2}/V^2\right)^2 + 1}$$
$$\approx 0.00067\ \text{m}^2\ \text{s}^{-2}/V^2 + 0.0001, \quad (2)$$

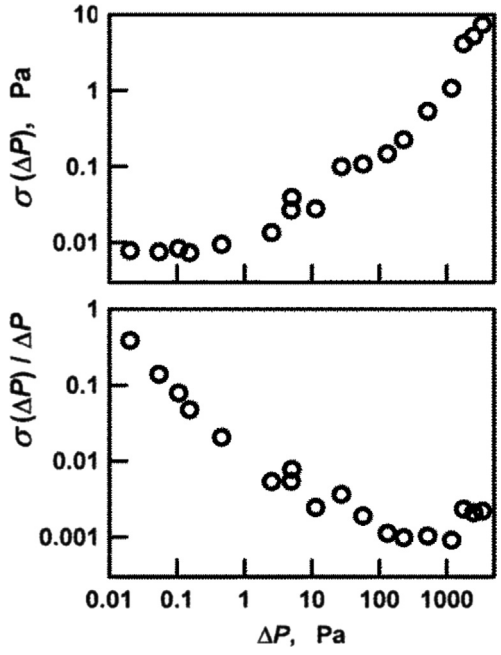

Fig. 13. Top: Fluctuations of differential pressure ΔP from. its mean value as a function of the pressure. Bottom: Relative pressure fluctuations.

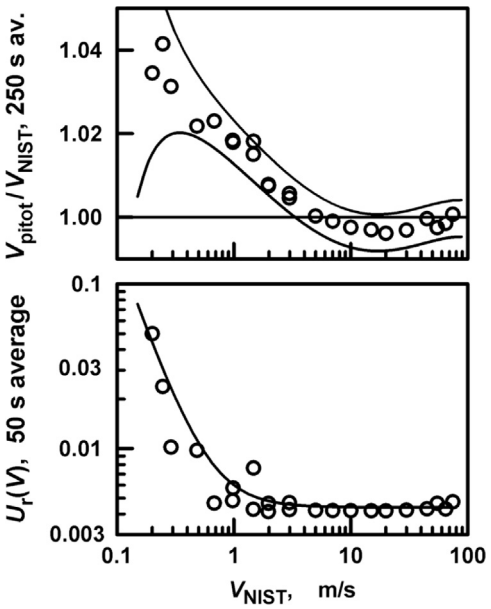

Fig. 14. Top: Calibration data for a Pitot tube. The curved lines indicate the $k=2$ uncertainty expected when 5 independent values of $V_{\text{Pitot}}/V_{\text{NIST}}$ are averaged at each air-speed. (V_{Pitot} is the air speed deduced from the pressure difference measured using a pitot tube; V_{NIST} is the air speed measured with the LDA.) Bottom: Relative expanded ($k=2$) uncertainty of a calibrated pitot tube as a function of air speed. Eq. (3) is plotted as a solid curve.

where the approximation in Eq. (2) is within the scatter of the data in Fig. 13.

For most customer calibrations, we use NIST-calibrated Pitot tubes as working standards and as check standards. The calibration of a Pitot tube has an uncertainty contribution from ΔP given by Eq. (2) and an additional uncertainty contribution $u_{\text{LDA}}(V) = 0.0022$ m/s from the laser Doppler anemometer, as discussed above in connection with Fig. (6). Therefore, the relative expanded uncertainty of a Pitot tube calibration with coverage factor $k=2$ is

$$U_r(V) = \frac{0.0013\ \text{m}^2/s^2}{V^2} + 0.0044 \quad (3)$$

The top panel of Fig. 14 displays real calibration data. Five 50 s long measurements were made at each value of V_{NIST} and averaged. At low air speeds, where pressure fluctuations dominate the uncertainty of $v_{\text{Pitot}}/V_{\text{NIST}}$, the averaging halved the uncertainty predicted by Eq. (3). The solid curves in the top panel of Fig. (14) indicate the expected uncertainty after averaging.

11. Controls and data acquisition

We implemented automated air-speed control in NIST's air speed calibration facility. This innovation significantly improved the precision, repeatability, and flexibility of customer calibrations and it reduced the chances of an operator error. The control system includes a low noise modified digital PID algorithm [9] that provides both rapid set point approach and low noise control at the target air speed. A user-selectable option will automatically fine tune the PID parameters used at each target air speed. Without operator intervention, the system sets air speeds at user-designated values with a repeatability of 0.05% or less. Before automation, the operator set a desired air speed by adjusting the power driving the wind tunnel's fan. This manual, iterative, process was time consuming and it reproduced targeted air speeds with a tolerance of 1% at best.

The PID and stability monitoring capability has also allowed the expansion of what was a single run operation into a system that can perform multiple measurement runs using complex, stepped air-speed-vs-time profiles. Typical, unattended runs can contain *hundreds of air speed steps and can take from several* hours to more than a day to complete. Before this control software was developed, it was not practical, and in many cases not possible, to perform tests involving extensive, complex air speed profiles or to run multiple tests at extremely low air speeds.

We are exploiting the capability for long, unattended runs to characterize multi-hole (3-D) Pitot tubes. [10] To do so, we measure the differential pressures between several pressure taps at multiple pitch and yaw angles and at multiple air speeds. Thus hundreds or thousands of measurements are collected to characterize a single 3-D Pitot tube.

The data acquisition and control program was written at NIST using National Instruments LabVIEW-FDS software. The program was developed using a queue-based state machine architecture that includes both user event driven and software timed state control. System environmental sensors, air speed measurement instruments, and instruments under test (IUTs) are continuously monitored at a rate of 10 Hz. All readings, instantaneous and averaged, of raw measurement data and conditioned velocity readings are available for display on the user interface using a multilayer tab display structure.

Display tabs are available for all instruments in the top center of the display. A set of secondary control tabs in the lower center of the display are used for PID and auxiliary instrument monitoring and control. On the left is a set of always visible system controls, and on the right, a set of always visible system and sensor status indicators.

An additional tab structure is used to selectively display sets of controls and indicators for other instruments such as the Dantec and Artium LDAs, the Vaisala and Fluke environmental monitoring instruments, and the control panel for the stability criteria and PID control parameter settings. Master air speed system controls, such as those used to select manual or automatic run mode, data collection state, LDA particulate seeding level, and emergency system stop, are always displayed on the user interface. During a data acquisition run, final averaged data readings for each air speed setting are collected and written to disk. There is also a manual option to collect bursts of high speed data for individual sensors, which has been useful in the study turbulent flows.

The control program uses a number of different communication interfaces to acquire data and control the air speed system. Pressure-based instrument readings are acquired using a PCI-based multifunction DAQ board, while auxiliary LabVIEW[1] programs are used to continuously monitor Laser Doppler Anemometers, the environmental sensors, (temperature, pressure, and relative-humidity) and additional auxiliary instruments. Ethernet, GPIB, and RS-232 serial interfaces are used to communicate with these external devices. Additional serial interfaces are used to control the wind tunnel recirculating fan power level and the LDA seeding motor.

12. Optical character recognition

Approximately 1/4 of the instruments submitted to NIST's Air Speed Calibration Service for calibration do not have electrical outputs or communication interfaces that can transfer the instrument's readings to a data-acquisition computer. In the past, an operator manually recorded the data generated during the calibration of these instruments and then entered the data into a spreadsheet for analysis. Now, NIST uses a LabVIEW-based optical character recognition (OCR) program module to transfer data from such instruments to a computer. The OCR module uses an inexpensive HD webcam to continuously monitor digital displays at rates up to 30 Hz, captures the displayed images, and converts them it into ASCII numeric values.

Before using the OCR module, setup procedures must be followed, including: camera setup, image tuning, and character training. The camera setup optimizes the camera position, lighting, focus, and image enhancement to provide high-quality images. Once the camera image has been optimized, the OCR program uses an automatic or manual image contrast threshold procedure to create a sharply defined 1 bit black and white image. If necessary, image noise reduction algorithms can be applied to remove unwanted image artifacts. The program then parses a user selected area within the image into individual character blocks. An image ratio quality matching is then applied to each block to find the best character match from within a selected font database. The font database used in the program is either loaded from an existing library of font files or created using character ID training and editing options built into the module. When using the built-in training option, the font database is automatically updated as new character images are captured in a training session. Image setup and tuning parameters can also be saved for each type of instrument, creating a library of pre-defined instrument specific image settings that can be recalled when needed. Once the setup and font database have been loaded or defined for an instrument, the OCR module runs without further user interaction, providing continuously updated readings from the monitored instrument.

Table 1
Uncertainty budget of the LDA (secondary standard) air speed measurement.

	Variable sources	Source description	Speed uncertainty		
			Mean	u_A (%)	u_B (%)
LDA calibration uncertainty	Disk	Diameter of the disk (mm)	136.526	0	0.0037
	LDA calibration	Calibration factor for speeds in the range from 0.2 m/s to 10 m/s	1.0024	0.205	0
	Misalignment of the disk against LDA	*X*-coordinate			3.0E-05
		Y-coordinate			0.027
		Z-coordinate			0
		Disk and beams planes			0.015
	Thermal expansion of the disk	Material of the disk			0.0049
	Thermal expansion of the beams' spacing	Material of the LDA probe			0.0049
LDA installation uncertainty	Thermal expansion of the beams' spacing	Material of the LDA probe			0.0049
	Misalignment of the disk against LDA	Pitch			0.015
		Yaw			0.015
BSA	BSA	Internal clock			0.00010
Root sum squares					0.205
$k=2$ uncertainty					0.41

13. Uncertainty of LDA standard

Table 1 is an uncertainty budget for the LDA secondary standard over the range of 0.2–10 m/s. In addition to the major sources of uncertainty discussed above, Table 1 includes minor, type B uncertainties from the thermal expansion of the disk and of the LDA probe, various misalignments, and the frequency. Consistent with Table 1, two calibrations conducted three months apart differed by only 0.16% and both had the same Type A uncertainty. Table 1 omits uncertainties from LDA misalignment, rotation dependence of the shape of the wire and imperfect tracking of the velocity by oil droplets. These effects are less than $1/3^{rd}$ of the uncertainties tabulated, as discussed in [1].

14. Conclusions

We greatly improved the performance and the flexibility of NIST's Air Speed Calibration Facility. The improved procedures for calibrating the secondary standard (LDA) against NIST's spinning disk reduced the uncertainty of the LDA from 1.4% to 0.42% at air speeds below 0.5 m/s. We eliminated windows corrections to the LDA calibration factor by permanently fixing the position of the LDA's sensing volume. Now, the calibration procedures for almost for all types of air speed instruments are automated. We calibrate most customers' instruments using, as a tertiary standard, a Pitot tube together with well-characterized differential pressure gauges. At low air speeds, this change reduced the uncertainty of the calibrations by 50%, provided that the calibrated instruments have sufficient stability. In the future, we will discuss the effects of blockage on calibrations conducted in NIST's wind tunnel.

References

[1] Yeh TT, Hall. JM. Airspeed calibration service. (SP250-79). NIST Special Publication; 2007.
[2] Shinder II, Hall JM, Moldover. MR. Improved airspeed calibration facility. In: Measurement science conference; 2010. (Published on disk).
[3] Spazzini PG, Piccato A, Malvano R. Metrological features of the linear low-speed anemometer calibration facility at INRIM. Metrologia 2009;46:109–18.
[4] Ower E, Jonansen FC, Mech AM. On a determination of the Pitot-static tube factor at low reynolds numbers, with special reference to the measurement of low air speeds. Proc R Soc Lond Ser A 1932;136(829):153–75.
[5] Bean VE, Hall JM. New primary standard for airspeed measurement at NIST. In: Proceedings of the NCSL workshop and symposium; 1999. p.413.
[6] Shinder II, Moldover MR, Hall JM, Duncan M, Keck J. Airspeed calibration services: laser doppler anemometer calibration and its uncertainty. In: Proceedings of the 8th international symposium on fluid flow measurements; 2012.
[7] Kurihara N, Terao Y, Takamoto M. LDV calibrator for the air speed standard between 1.3 and 40 m/s. In: Proceedings of the 5th international symposium on fluid flow measurement. Arlington, Virginia; April 2002.
[8] Becker HA, Brown. APG. Response of Pitot probes in turbulent streams. Fluid Mech 1974;62:85–114 (Part 1).
[9] Hust JG, Filla BJ, Smith. DR. A Modified Digital PID Temperature Controller for Thermal Properties Measurements. J Therm Insul 1987;11:102.
[10] Crowley C, Shinder II, Moldover MR. The effect of turbulence on a of multi-hole Pitot calibration. Flow Meas Instrum 2013;33:106–9.